# Technical Note: Multiple wavelet coherence for untangling scale-specific and localized multivariate relationships in geosciences

Wei Hu[2,3] and Bing Cheng Si[1,3]

[1]*College of Hydraulic and Architectural Engineering, Northwest A&F University, Yangling 712100, China*

[2]*New Zealand Institute for Plant & Food Research Limited, Private Bag 4704, Christchurch 8140, New Zealand*

[3]*University of Saskatchewan, Department of Soil Science, Saskatoon, SK S7N 5A8, Canada*

*Correspondence to:* Wei Hu (wei.hu@plantandfood.co.nz) and Bing Cheng Si (bing.si@usask.ca)

## Abstract

The scale-specific and localized bivariate relationships in geosciences can be revealed using bivariate wavelet coherence. The objective of this study was to develop a multiple wavelet coherence method for examining scale-specific and localized multivariate relationships. Stationary and non-stationary artificial datasets, generated with the response variable as the summation of five predictor variables (cosine waves) with different scales, were used to test the new method. Comparisons were also conducted using existing multivariate methods, including multiple spectral coherence and multivariate empirical mode decomposition (MEMD). Results show that multiple spectral coherence is unable to identify localized multivariate relationships, and underestimates the scale-specific multivariate relationships for non-stationary processes. The MEMD method was able to separate all variables into components at

the same set of scales, revealing scale-specific relationships when combined with multiple correlation coefficients, but has the same weakness as multiple spectral coherence. However, multiple wavelet coherences are able to identify scale-specific and localized multivariate relationships, as they are close to 1 at multiple scales and locations corresponding to those of predictor variables. Therefore, multiple wavelet coherence outperforms other common multivariate methods. Multiple wavelet coherence was applied to a real dataset and revealed the optimal combination of factors for explaining temporal variation of free water evaporation at Changwu site in China at multiple scale-location domains. Matlab codes for multiple wavelet coherence were developed and are provided in the supplement.

## 1. Introduction

Geoscience data such as topography, climate, and ocean waves usually present cyclic patterns, with high-frequency (small-scale) processes being superimposed on low-frequency (large-scale) processes (Si, 2008). More often than not, geoscience data are transient, consisting of a variety of frequency regimes that may be localized in space or time (Torrence and Compo, 1998; Si and Zeleke, 2005; Graf et al., 2014). The transient characteristics exist widely in non-stationary processes, but also sometimes occur in stationary processes (Feldstein, 2000). The wavelet method is a common tool for detecting multi-scale and localized features of transient processes in geosciences. Bivariate wavelet coherency has been widely used for untangling scale-specific and localized relationships for transient processes in areas including

geophysics (Lakshmi et al., 2004; Müller et al., 2008), hydrology (Labat et al., 2005; Das and Mohanty, 2008; Tang and Piechota, 2009; Carey et al., 2013; Graf et al., 2014), soil science (Si and Zeleke, 2005; Biswas and Si, 2011), meteorology (Torrence and Compo, 1998), and ecology (Polansky et al., 2010). This method, however, is limited to two variables. Processes in geosciences are usually complex and may be affected by more than two environmental factors. A method is needed for analyzing multivariate (>2 variables) and localized relationships at multiple scales.

Several methods have been used for characterizing multivariate relationships. For example, multiple spectral coherence (MSC) has been used to explore the scale-specific relationships between soil saturated hydraulic conductivity ($K_s$) and multiple soil physical properties (Koopmans, 1974; Si, 2008), but requires a stationary data series, which is rare in geosciences. Multivariate empirical mode decomposition (MEMD), a data-driven method, decomposes each variable into different components (intrinsic mode functions (IMFs)) with each IMF corresponding to a "common scale" inherent in multiple variables (Rehman and Mandic, 2010). The MEMD method is meritorious due to its ability to deal with both transient and nonlinear systems. The combination of the squared multiple correlation coefficient and MEMD ($MCC_{memd}$) has been used to explore the multivariate control of soil water content and $K_s$ at multiple scales (Hu and Si, 2013; She et al., 2013, 2015; Hu et al., 2014). However, the sum of variances from different components did not typically equal the total variance of the original series, which may produce misleading $MCC_{memd}$ results. In addition, multivariate relationships in geosciences are most likely to change with time

or space due to the transient nature of the processes involved. However, localized multivariate relationships are not available using any of the existing multivariate methods. Therefore, extending the wavelet coherence from two variables to multiple variables is required .

An attempt to extend wavelet coherence from two to three variables has been made by Mihanović et al. (2009). Their method was also applied later in the marine sciences (Ng and Chan, 2012a, b). Limitations arise when using the trivariate wavelet coherence: first, only two predictor variables are considered; second, the two predictor variables must be orthogonal. Otherwise, extremely high or low (spurious) coherence (>>1 or <0) may be produced. This spuriousness is inconsistent with the definition of coherence, which may limit the application of this method in geosciences where environmental variables are usually cross-correlated. Therefore, a robust method for calculating MWC, which produces coherence in the closed interval of [0, 1], is needed.

The objective of this paper is to develop an MWC that applies to cases where there are multiple environmental variables, of which may be cross-correlated. This method is first tested with artificial datasets to demonstrate its advantages over existing multivariate methods. The superiority of the new method over others can be assessed by determining whether the known major features of the artificial data are demonstrated by these methods. The new method is then applied to a temporal series of evaporation ($E$) from free water surface and meteorological factors at Changwu site in Shaanxi, China.

## 2. Theory

Bivariate wavelet coherence can be understood as the traditional correlation coefficient localized in the scale-location domain (Grinsted et al., 2004). Just as correlation coefficients can be extended from two variables to multiple (>2) variables, wavelet coherence between two variables may also be extended to multiple variables. Similar to bivariate wavelet coherence, MWC is based on a series of auto- and cross-wavelet power spectra, at different scales and spatial (or temporal) locations, for the response variable and all predictor variables.

Following Koopman (1974), a matrix representation of the smoothed auto- and cross-wavelet power spectra for multiple predictor variables $X$ ( $X = \left\{ X_1, X_2, \ldots, X_q \right\}$ ) can be written as

$$\overleftrightarrow{W}^{X,X}(s,\tau) = \begin{bmatrix} \overleftrightarrow{W}^{X_1,X_1}(s,\tau) & \overleftrightarrow{W}^{X_1,X_2}(s,\tau) & \cdots & \overleftrightarrow{W}^{X_1,X_q}(s,\tau) \\ \overleftrightarrow{W}^{X_2,X_1}(s,\tau) & \overleftrightarrow{W}^{X_2,X_2}(s,\tau) & \cdots & \overleftrightarrow{W}^{X_2,X_q}(s,\tau) \\ \vdots & \vdots & & \vdots \\ \overleftrightarrow{W}^{X_q,X_1}(s,\tau) & \overleftrightarrow{W}^{X_q,X_2}(s,\tau) & \cdots & \overleftrightarrow{W}^{X_q,X_q}(s,\tau) \end{bmatrix}, \quad (1)$$

where $\overleftrightarrow{W}^{X_i,X_j}(s,\tau)$ is the smoothed auto-wavelet power spectra (when $i=j$) or cross-wavelet power spectra (when $i \neq j$) at scale $s$ and spatial (or temporal) location $\tau$, respectively. For the detailed calculation of smoothed auto- and cross-wavelet power spectra, see Supplement, Sect. S1.

The matrix of smoothed cross wavelet power spectra between response variable $Y$ and predictor variables $X_i$ can be defined as

$$\overleftrightarrow{W}^{Y,X}(s,\tau) = \left[ \overleftrightarrow{W}^{Y,X_1}(s,\tau) \;\; \overleftrightarrow{W}^{Y,X_2}(s,\tau) \cdots \overleftrightarrow{W}^{Y,X_q}(s,\tau) \right], \quad (2)$$

where $\overleftrightarrow{W}^{Y,X_i}(s,\tau)$ is the smoothed cross-wavelet power spectra between $Y$ and $X_i$ at scale $s$ and spatial (or temporal) location $\tau$.

The smoothed wavelet power spectrum of response variable $Y$ is $\overleftrightarrow{W}^{Y,Y}(s,\tau)$.

Following Koopmans (1974), the MWC at scale $s$ and location $\tau$, $\rho_m{}^2(s,\tau)$, can be written as

$$\rho_m{}^2(s,\tau)=\frac{\overleftrightarrow{W}^{Y,X}(s,\tau)\overleftrightarrow{W}^{X,X}(s,\tau)^{-1}\overline{\overleftrightarrow{W}^{Y,X}(s,\tau)}}{\overleftrightarrow{W}^{Y,Y}(s,\tau)}. \quad (3)$$

When only one predictor variable (e.g., $X_1$) is included in $X$, Eq. (3) is the equation for bivariate wavelet coherence, $\rho_b^2(s,\tau)$, which can be expressed as (Torrence and Webster, 1999; Grinsted et al., 2004):

$$\rho_b^2(s,\tau)=\frac{\overleftrightarrow{W}^{Y,X_1}(s,\tau)\,\overline{\overleftrightarrow{W}^{Y,X_1}(s,\tau)}}{\overleftrightarrow{W}^{X_1,X_1}(s,\tau)\overleftrightarrow{W}^{Y,Y}(s,\tau)}. \quad (4)$$

Therefore, bivariate wavelet coherence is consistent with multiple wavelet coherence if only one predictor variable is included. In addition, the wavelet phase between a response variable ($Y$) and a predictor variable ($X_1$) is

$$\phi(s,\tau)=\tan^{-1}\left(\mathrm{Im}\left(W^{Y,X_1}(s,\tau)\right)/\mathrm{Re}\left(W^{Y,X_1}(s,\tau)\right)\right), \quad (5)$$

where Im and Re denote the imaginary and real part of $W^{Y,X_1}(s,\tau)$, respectively. Note that the phase information between a response variable $Y$ and multiple predictor variables $X$ cannot be obtained.

Multiple wavelet coherence at the 95% confidence level is calculated using the Monte Carlo method (Grinsted et al., 2004). Surrogate spatial series (i.e., red noise) of all variables are generated with a Monte Carlo simulation based on their first-order autocorrelation coefficient (AR1). The MWC at each scale and location is calculated

using the simulated spatial series. This is repeated an adequate number of times (e.g., 1000) (Grinsted et al., 2004). At each scale, MWCs at all locations outside the cones of influence, from all simulations are ranked in ascending order. The value at the 95th percentile represents the 95% confidence level for the MWC at that scale. The Matlab codes and user manual document for calculating MWC and significance level are provided in the Supplement (Sect. S2–S4).

# 3. Data and analysis

## 3.1 Artificial data for method test

The method is tested using a stationary and non-stationary artificial dataset, generated following Yan and Gao (2007). The response variable ($y$ for the stationary case and $z$ for the non-stationary case) encompasses five cosine waves ($y_1$ to $y_5$ for the stationary case and $z_1$ to $z_5$ for the non-stationary case), with different dimensionless scales (Fig. 1). For the stationary case, $y_1=\cos(2\pi x/4)$, $y_2=\cos(2\pi x/8)$, $y_3=\cos(2\pi x/16)$, $y_4=\cos(2\pi x/32)$, and $y_5=\cos(2\pi x/64)$, where $x$=0, 1, 2, …, 255. There is one regular cycle every 4, 8, 16, 32, and 64 locations, representing dimensionless scales of 4, 8, 16, 32, and 64 for $y_1$, $y_2$, $y_3$, $y_4$, and $y_5$, respectively (Fig. 1a). The regular cycles make each predictor and response series stationary. For the non-stationary case, $z_1=\cos(500\pi(x/1000)^{0.5})$, $z_2=\cos(250\pi(x/1000)^{0.5})$, $z_3=\cos(125\pi(x/1000)^{0.5})$, $z_4=\cos(62.5\pi(x/1000)^{0.5})$, and $z_5=\cos(31.25\pi(x/1000)^{0.5})$, where $x$=0, 1, 2, …, 255. The equation containing the square root of the location term results in the gradual change in frequency (scale), with the greatest dimensionless scales of 4, 8, 16, 32, and 64 at

148 the right hand side for $z_1$, $z_2$, $z_3$, $z_4$, and $z_5$, respectively (Fig. 1b). The average scales
149 for these predictor variables are 3, 5, 9, 17, and 32, respectively. The location-varying
150 scales make each predictor and response variable non-stationary.

151 For both the stationary and non-stationary series, the variance of the response
152 variable is 2.5. The predictor variables, each with a variance of 0.5, are orthogonal to
153 each other, and contribute equally to the total variance of the response variable. The
154 cosine-like artificial datasets mimic many time series such as seismic signals,
155 turbulence, air temperature, precipitation, hydrologic fluxes, and the El
156 Niño-Southern Oscillation. They also mimic geoscientific spatial series such as ocean
157 waves, seafloor bathymetry, land surface topography, and soil water content along a
158 hummocky landscape. Therefore, they are representative of a geoscience data series
159 and are suitable for testing the new method.

160 Multiple wavelet coherence between the response variable $y$ (or $z$) and two ($y_2$ and
161 $y_4$, or $z_2$ and $z_4$) or three ($y_2$, $y_3$, and $y_4$, or $z_2$, $z_3$, and $z_4$) predictor variables were
162 calculated. The advantage of the artificial data is that the known scale- and localized
163 features for all variables, and the known relationships between the response and each
164 predictor variable, are exact. By definition, the coherence is 1 at scales corresponding
165 to those of the included predictor variables, and 0 at other scales.

166 To demonstrate the advantages of MWC in dealing with abrupt changes (a type of
167 transient and localized feature), the second half of the original series of $y_2$ (or $z_2$) or $y_4$
168 (or $z_4$) are replaced by 0, and MWC between the response variable and new set of
169 predictor variables is calculated. We anticipate that the coherence changes from 1 to 0

170 at the location where the new predictor variable becomes 0.

171 Predictor variables may not be as regular as that shown in Fig. 1, and may also be
172 cross-correlated to one another. For these reasons, zero-mean white noises with
173 standard deviations of 0.3, 1, and 4 are added to the predictor variables of $y_2$ (or $z_2$)
174 and $y_4$ (or $z_4$). The resulting noised series have correlation coefficients of 0.9, 0.5, and
175 0.1, respectively, with their original predictor variable. Therefore, we will refer to
176 them as weakly, moderately, and highly noised series, respectively. Multiple wavelet
177 coherences between the response variable and different predictor variables (original
178 and noised series) are calculated to demonstrate the performance of MWC when
179 noised or correlated predictor variables are involved. Only the non-stationary case
180 will be demonstrated, because the performances of MWC for stationary and
181 non-stationary cases are similar.

182 The MWC is compared to the MSC (Koopmans, 1974; Si, 2008) and $MCC_{memd}$ (Hu
183 and Si, 2013), which are widely used for spatial or temporal series analysis in
184 different disciplines. The advantages of the new method over these two methods will
185 be demonstrated mainly in terms of relationships between response and predictor
186 variables at various scales of the response variable. The MSC is calculated based on
187 the calculated auto- and cross- power spectra, using an equation similar to Eq. (3).
188 The detailed introduction of this method can be found in Si (2008). For the calculation
189 of $MCC_{memd}$, a set of response and predictor variables form a multivariate data series
190 for MEMD. The MEMD is a data driven method and has the ability to align “common
191 scales” present within multivariate data. Please refer to Rehman and Mandic (2010)

and Hu and Si (2013) for the MEMD analysis, and the website (http://www.commsp.ee.ic.ac.uk/~mandic/research/emd.htm) for the related Matlab codes. The original series of response and predictor variables can be decomposed by the MEMD, into different components (IMFs) with varying scales. For IMFs at the same scale, multiple stepwise regressions are conducted between response and predictor variables, and the multiple correlation coefficients for each scale-specific IMF are calculated.

### 3.2 Real data for application

Daily evaporation (*E)* from free water surfaces in an E601 evaporation pan (pan diameter of 61.8 cm), and other meteorological factors (i.e., relative humidity, mean temperature, sun hours, and wind speed) were collected from January 1, 1979 to December 31, 2013, at Changwu site in Shaanxi, China. The Changwu site is a transition area between semi-arid and subhumid climates, where agricultural productivity is mainly limited by water. Monthly averages of all variables were used in this study, because we are mainly interested in seasonal and inter-annual variability.

## 4. Results and discussion

### 4.1 MWC with orthogonal predictor variables

For the stationary data, there are two narrow, horizontal bands (red color) representing an MWC value of around 1, at the respective scales of 8 and 32 for all locations (Fig. 2a). These two bands also correspond to the scales of 8 and 32,

212 respectively, for the two predictor variables. When an additional predictor variable
213 with the scale of 16 is introduced, a wide band appears from 6 to 40, signifying that
214 the MWC equals approximately 1 at all locations, at the scales of 8, 16, and 32. As
215 anticipated, when all five predictor variables with scales ranging from 4 to 64 are
216 included, coherence values of close to 1 are found in the whole scale-location domain
217 (data not shown).

218 The application of MWC to the non-stationary datasets shows that the scales with
219 significant MWC values gradually increase as distance increases. This increase in the
220 scales is due to the non-stationarity of the variables (Fig. 2b). For example, when
221 predictor variables of $z_2$ and $z_4$ are included, scales of the two bands corresponding to
222 MWC around 1 increase from 4 to 8 and from 8 to 32, respectively. Furthermore, as
223 expected, for only one predictor variable (stationary and non-stationary), MWC
224 reduces to bivariate wavelet coherence; there is only one band of coherence around 1,
225 which corresponds to the scale of that predictor variable (data not shown). Note that
226 the significant MWC values for both stationary and non-stationary cases are not
227 exactly 1 at all scales or locations, due to the smoothing effect along both scales and
228 locations. However, the mean MWC values of the significant bands are very high (i.e.,
229 0.94–1.00), and the MWC values at the centre of the significant band are 1, which
230 corresponds to the exact scale of a predictor variable.

231 When the point values in the second half of the data series of a predictor variable
232 are replaced by 0, the MWC values in that half of the data series are almost 0 at scales
233 corresponding to that predictor variable (Fig. 3). For the stationary case, when the

point values in the second half of the data series of predictor variable $y_2$ (or $y_4$) are replaced by 0, the MWC values are around 1 at the scale of 8 (or 32) in the first half of the transect, and 0 in the second half (Fig. 3a). Similar results are also found for the non-stationary case (Fig. 3b). This is expected because the constant series of 0 is not correlated to the response variables at any scale. Much like bivariate wavelet coherence, the MWC method is able to detect abrupt changes in the data series, and has the advantages of dealing with localized multivariate relationships.

### 4.2 MWC with noised and correlated predictor variables

When $z_2$ and a noised series derived from $z_2$ are included as predictor variables, there is only one band of coherence close to 1 at scales corresponding to $z_2$, irrespective of the correlation between $z_2$ and a noised series of $z_2$ (Fig. 4a). When $z_2$ and a noised series of $z_4$ are included as predictor variables, the coherence depends on the degree of the noise (Fig. 4b). For weakly noised series, there are two bands of coherence of around 1, corresponding to the scales of $z_2$ and $z_4$, respectively. The percentage area of significant coherence (PASC) is 23%, which equals that of when $z_2$ and $z_4$ are included. With the increasing magnitude of noise, the coherence and corresponding PASC at the scales corresponding to $z_4$ decrease. When $z_2$ and a strongly noised series of $z_4$ are considered, the band of coherence around 1, at scales corresponding to $z_4$, disappears.

The inclusion of a third noised $z_4$ variable substantially increases the area with high coherence (in red) as compared to the case when only $z_2$ and $z_4$ are included (Fig. 4c).

This indicates that MWC will increase as the number of predictor variables increases, with the highest coherence less or equal to 1, irrespective of the number of predictor variables. However, the area of significant coherence may not necessarily increase because of the simultaneously increased statistical significance threshold (Ng and Chan, 2012a). In fact, the PASC values for three predictor variables (19–20%) are lower than those of the two predictor variables (23%). This indicates that, in this case, two predictor variables are better than three in terms of explaining the variations of the response variable. This occurs because the variance of the response variable that is explained by the noised variable is already accounted for by other variables. Therefore, only an additional variable that can independently explain a fair amount of variance could contribute significantly to explaining variations of a response variable (Fig. 4b). This may also explain why there is only one band of coherence around 1 at scales corresponding to $z_2$, when $z_2$ and a noised series of $z_2$ are included (Fig. 4a). This information is helpful in choosing predictor variables for developing scale-specific predictions, especially when predictor variables are correlated.

## 4.3 Comparison with other multivariate methods

### 4.3.1 MSC

The MSC as a function of scale is shown in Fig. 5a. For the stationary case, when $y_2$ and $y_4$ are included as predictor variables, there are two plateaus centered at the scales of 8 and 28, representing a coherence of 1. As expected, when an additional predictor variable $y_3$ is added, the corresponding scale of 16 also shows coherence of

1. The MSC produces similar scale-specific relationships, as MWC does for a stationary dataset, with exception given to the centered scale (i.e., 28) with a coherence of 1. Here, the scale with a unity MSC deviates from the expected value (i.e., 32) for predictor variable $y_4$. For the non-stationary case, however, the MSC is much lower than 1 for the predictor variables of $z_2$ and $z_4$; an MSC of 1 is present only at the scale of 8 when an additional predictor variable $z_3$ is added. Obviously, the MSC underestimates the multivariate relationships, and is not suitable for non-stationary processes (Si, 2008) due to its inability to deal with localized features. The MSC at a specific scale provides the average of multivariate relationships, across all locations. Due to the change in scale of a predictor variable with location for the non-stationary case, the MSC deviates greatly from 1.

The MSC decreases at scales when the second half of the included predictor variable series are replaced by 0 for both the stationary and non-stationary series (Fig. 5b). For example, when the second half of the $y_4$ series in the stationary case are replaced by 0, the MSC at scales of around 32 decreases from 1 to 0.52. Although the MSC, throughout the second half of the series, can detect the decrease of coherence at the scales corresponding to the 0 values, the exact locations for the decrease cannot be identified. In fact, the coherence decreases only in the second half of the series, and does not change in the first half of the series. The location for the decrease can be easily identified by the MWC, but not by MSC. This further demonstrates the inability of the MSC to deal with localized features.

297 4.3.2 $MCC_{memd}$

298 Five intrinsic mode functions (IMFs) with non-negligible variance, are obtained for
299 multivariate data series. While the obtained scales for the response variable *y* are in
300 agreement with the true scales for the stationary case, the obtained scales (i.e., 3, 6, 11,
301 21, and 43) for the response variable *z* deviate slightly from the average scales for the
302 non-stationary case. For the response variable, the contribution of IMFs to the total
303 variance generally decreases (20% to 13% for stationary, and 27% to 11% for
304 non-stationary) from IMF1 to IMF5. This disagrees with the fact that each scale
305 contributes equally (i.e., 20%) to the total variance. In addition, the sum of variances
306 over all IMFs for each variable is less than 100% (ranging from 84% to 93%),
307 indicating that MEMD cannot capture all the variances. For the detailed results of
308 MEMD, see Supplement, Sect. S5.

309 The $MCC_{memd}$ as a function of scale, is shown in Fig. 6a. For the stationary case,
310 when predictor variables of $y_2$ and $y_4$ are included, the $MCC_{memd}$ values are 0.98 and
311 0.93, respectively, at scales corresponding to those of $y_2$ and $y_4$. When a predictor
312 variable of $y_3$ is included, the $MCC_{memd}$ values are 1.00, 1.00, and 0.96, respectively,
313 at scales corresponding to those of $y_2$, $y_3$, and $y_4$. For the non-stationary, two predictor
314 variable case, the corresponding $MCC_{memd}$ values are 0.80 and 0.85. For the
315 non-stationary, three predictor variable case, the corresponding $MCC_{memd}$ values are
316 0.95, 0.99, and 0.91, respectively. Therefore, the $MCC_{memd}$ can be used to determine
317 the scale-specific multivariate relationships. Similar to MSC, however, the $MCC_{memd}$
318 underestimates the multivariate relationships, especially for the non-stationary case

with less predictor variables. On the contrary, the $MCC_{memd}$ also overestimates the multivariate relationships. For example, when considering only predictor variables corresponding to scales of 8, 16, and 32, the $MCC_{memd}$ value for the stationary case is 0.47 at the scale of 64. This deviates much from the expected $MCC_{memd}$ value of 0 (Fig. 6a). The possible underestimation and overestimation by the $MCC_{memd}$ may come from the decomposition errors inherent in the MEMD algorithm (Rehman and Mandic, 2010).

Similar to MSC, the localized multivariate relationships cannot be obtained from $MCC_{memd}$. This can be better explained by the decrease of $MCC_{memd}$ when half of the series of the predictor variables are replaced by 0 (Fig. 6b). Take the stationary case for example, the $MCC_{memd}$ values at the scales corresponding to $y_2$ and $y_4$ decrease from 0.98 to 0.49, and from 0.93 to 0.62, respectively, when the second half of the $y_2$ and $y_4$ series are replaced by 0.

As explained above, the MWC has advantages in untangling localized multivariate relationships as compared to the common multivariate methods. It is important to reveal the multivariate relationships which vary with time or space, that are associated with different processes. For example, discharge usually occurs on knolls, while recharge usually occurs in neighboring depressions (Gates et al., 2011). Therefore, the controlling factors of soil water storage may vary with the land element characteristics of a location. Local controls may be more important on knolls, while non-local controls may be more important in depressions (Grayson et al., 1997). In a temporal domain, vegetation transpiration contributes more to the evapotranspiration in the

341 growing seasons, which may result in the changes of environmental factors explaining
342 temporal variations of evapotranspiration in different seasons.

343 **4.4 Application of the MWC**

344 Each meteorological factor was significantly correlated to *E*, but the dominant
345 factors explaining variations in *E* differed with scale. For example, the relative
346 humidity was the dominating factor at small (2–8 months) and large (>32 months)
347 scales, while temperature was the dominating factor at the medium (8–32 months)
348 scales. Overall, the relative humidity corresponded to the greatest mean MWC (0.62)
349 and PASC value (40%) at multiple scale-location domains. For the detailed
350 relationships between *E* and each factor, see Supplement, Sect. S6.

351 The MWC analysis shows that the combination of relative humidity and mean
352 temperature produced the greatest mean MWC (0.82) and PASC (49%) among all
353 two-factor cases. This suggested that relative humidity and mean temperature were
354 the most appropriate factors for explaining variations in *E* at multiple scale-location
355 domains (Fig. 7a). However, adding an additional factor such as sun hours, which was
356 the best among all three-factor cases, increased the average coherence (0.91), but
357 slightly decreased the PASC to 48% (Fig. 7b). This indicated that sun hours was not
358 significantly different from red noise in explaining additional variation in *E*. Similar
359 results were found when the wind speed was added. This occurs because most areas
360 with significant coherence between *E* and sun hours or wind speed were a subset of
361 areas with significant coherence between *E* and relative humidity or mean

362 temperature (see Supplement, Sect. S3). Therefore, relative humidity and mean
363 temperature were adequate for explaining the temporal variation of *E* at various scales
364 at this site. This was consistent with Li et al. (2012), who indicated that relative
365 humidity and mean temperature were the two main contributors to the temporal
366 change of potential evapotranspiration on the Chinese Loess Plateau.

367 **5. Conclusions**

368 Multiple wavelet coherence was developed to determine scale-specific and
369 localized multivariate relationships in geosciences. The new method was tested and
370 compared with existing multivariate methods, using an artificial dataset. The new
371 method can be used to determine the proportion of the variance of a response variable
372 that is explained by predictor variables, at a specific scale and location (spatially or
373 temporally). As compared with bivariate wavelet coherence, more variation may be
374 explained at multiple scale-location domains by the MWC. Including more variables
375 is only beneficial if the variables are not strongly cross-correlated, and can
376 independently explain a fair amount of variability in a response variable. Therefore,
377 the best combinations of variables that explain multivariate, spatial or temporal
378 variability at multiple scales can be determined. This is important for optimizing
379 variables to develop scale-specific prediction.

380 The MSC and $MCC_{memd}$ can determine multivariate relationships at multiple scales,
381 but localized multivariate relationships are not available. Furthermore, both MSC and
382 $MCC_{memd}$ are likely to underestimate the degree of multivariate relationships for

non-stationary processes. In addition, the performance of $MCC_{memd}$ relies on the performance of MEMD, which needs further development. Application of the MWC into the real dataset indicates that the combination of relative humidity and mean temperature are the optimal factors that can be used to explain temporal variations of *E* at the Changwu site in China.

Limitations of the new method also exist. Theoretically, any number of predictor variables can be included in the multiple wavelet analysis. However, the statistical significance threshold usually increases with the number of predictor variables (Grinsted et al., 2004; Ng and Chan, 2012a). In addition, the inclusion of too many predictor variables may result in the statistical significance threshold at particular wavelet scales (e.g., the lowest and largest scales) to approach unity. This would restrict the availability of statistical information. Furthermore, similar to bivariate wavelet analysis, the new method also suffers from the multiple-testing problem (Maraun and Kurths, 2004; Maraun et al., 2007; Schaefli et al., 2007; Schulte et al., 2015; Schulte, 2016). Therefore, a more robust statistical significance testing method may be beneficial to the new method.

In summary, multiple wavelet coherence has advantages over existing multivariate methods, and provides an effective vehicle for untangling complex spatial or temporal variability for multiple controlling factors at multiple scales and locations. It may also be used as a data-driven tool for modeling and predicting various processes in the area of geosciences, such as precipitation, drought, soil water dynamics, stream flow, and atmospheric circulation.

## Acknowledgements

The Matlab codes for calculating multiple wavelet coherence are developed based on the codes provided by A. Grinsted (http://www.glaciology.net/wavelet-coherence) and, together with the user manual, are available in the Supplement (Sect. S2-S4). The project was funded by the National Natural Science Foundation of China (41371233), the Natural Sciences and Engineering Research Council of Canada (NSERC), Agriculture Development Fund of Saskatchewan, and the New Zealand Institute for Plant & Food Research under the Land Use Change and Intensification programme. We thank the two anonymous reviewers for their constructive comments.

## References

Biswas, A. and Si, B. C.: Identifying scale specific controls of soil water storage in a hummocky landscape using wavelet coherency, Geoderma, 165, 50–59, doi: 10.1016/j.geoderma.2011.07.002, 2011.

Carey, S. K., Tetzlaff, D., Buttle, J., Laudon, H., McDonnell, J., McGuire, K., Seibert, J., Soulsby, C., and Shanley, J.: Use of color maps and wavelet coherence to discern seasonal and interannual climate influences on streamflow variability in northern catchments, Water Resour. Res., 49, 6194–6207, doi: 10.1002/wrcr.20469, 2013.

Das, N.N. and Mohanty, B. P.: Temporal dynamics of PSR-based soil moisture across spatial scales in an agricultural landscape during SMEX02: A wavelet approach, Remote Sens. Environ., 112, 522–534, doi:10.1016/j.rse.2007.05.007, 2008.

Feldstein, S. B.: The timescale, power spectra, and climate noise properties of

426 teleconnection patterns, J. Clim., 13, 4430–4440,
427 doi:10.1175/15200442(2000)0132.0.CO, 2000.
428 Gates, J. B., Scanlon, B. R., Mu, X. M., and Zhang, L.: Impacts of soil conservation
429 on groundwater recharge in the semi-arid Loess Plateau, China, Hydrogeol. J., 19,
430 865–875, 2011.
431 Graf, A., Bogena, H. R., Drüe, C., Hardelauf, H., Pütz, T., Heinemann, G., and
432 Vereecken, H.: Spatiotemporal relations between water budget components and soil
433 water content in a forested tributary catchment, Water Resour. Res., 50, 4837–4857,
434 doi:10.1002/2013WR014516, 2014.
435 Grayson, R. B., Western, A. W., Chiew, F. H. S., and Blöschl, G.: Preferred states in
436 spatial soil moisture patterns: local and nonlocal controls, Water Resour. Res., 33,
437 2897–2908, doi: 10.1029/97WR02174, 1997.
438 Grinsted, A., Moore, J. C., and Jevrejeva, S.: Application of the cross wavelet
439 transform and wavelet coherence to geophysical time series, Nonlinear Proc. Geoph.,
440 11, 561–566, 2004.
441 Hu, W., Biswas, A., and Si, B. C.: Application of multivariate empirical mode
442 decomposition for revealing scale- and season-specific time stability of soil water
443 storage, Catena, 113, 377–385, doi:10.1016/j.catena.2013.08.024, 2014.
444 Hu, W. and Si, B. C.: Soil water prediction based on its scale-specific control using
445 multivariate empirical mode decomposition, Geoderma, 193–194,180–188, doi:
446 10.1016/j.geoderma.2012.10.021, 2013.
447 Koopmans, L. H.: The spectral analysis of time series, Academic Press, New York,

448 1974.
449 Labat, D.: Recent advances in wavelet analyses: Part I. A review of concepts, J.
450 Hydrol., 314, 275–288, doi: 10.1016/j.jhydrol.2005.04.003, 2005.
451 Lakshmi, V., Piechota, T., Narayan, U., and Tang, C. L.: Soil moisture as an indicator
452 of weather extremes, Geophys. Res. Lett., 31, L11401, doi:10.1029/2004GL019930,
453 2004.
454 Li, Z., Zheng, F. L., and Liu, W. Z.: Spatiotemporal characteristics of reference
455 evapotranspiration during 1961–2009 and its projected changes during 2011–2099 on
456 the Loess Plateau of China, Agric. For. Meteorol., 154-155, 147–155,
457 doi:10.1016/j.agrformet.2011.10.019, 2012.
458 Maraun, D. and Kurths, J.: Cross wavelet analysis: significance testing and pitfalls,
459 Nonlin. Processes Geophys., 11, 505–514, doi: 10.5194/npg-11-505-2004, 2004.
460 Maraun, D., Kurths, J., and Holschneider, M.: Nonstationary Gaussian processes in
461 wavelet domain: synthesis, estimation, and significance testing, Phys. Rev. E., 75,
462 016707, doi:10.1103/PhysRevE.75.016707, 2007.
463 Mihanović, H., Qrlić, M., and Pasrić, Z.: Diurnal thermocline oscillations driven by
464 tidal flow around an island in the Middle Adriatic, J. Marine Syst., 78, S157–S168,
465 doi: 10.1016/j.jmarsys.2009.01.021, 2009.
466 Müller, W. A., Frankignoul, C., and Chouaib, N.: Observed decadal tropical
467 Pacific–North Atlantic teleconnections, Geophys. Res. Lett., 35, L24810,
468 doi:10.1029/2008GL035901, 2008.
469 Ng, E. K. W. and Chan, J. C. L.: Geophysical applications of partial wavelet

coherence and multiple wavelet coherence, J. Atmos. Ocean. Tech., 29, 1845–1853, doi: 10.1175/JTECH-D-12-00056.1, 2012a.

Ng, E. K. W. and Chan, J. C. L.: Interannual variations of tropical cyclone activity over the north Indian Ocean, Int. J. Climatol., 32, 819–830, doi: 10.1002/joc.2304, 2012b.

Polansky, L., Wittemyer, G., Cross, P. C., Tambling, C. J., and Getz, W. M.: From moonlight to movement and synchronized randomness: Fourier and wavelet analyses of animal location time series data, Ecology, 91, 1506–1518, doi: 10.1890/08-2159.1, 2010.

Rehman, N. and Mandic, D. P.: Multivariate empirical mode decomposition, Proc. R. Soc. A., 466, 1291–1302, doi:10.1098/rspa.2009.0502, 2010.

Schaefli, B., Maraun, D., and Holschneider, M.: What drives high flow events in the Swiss Alps? Recent developments in wavelet spectral analysis and their application to hydrology, Adv. Water Resour., 30, 2511–2525, doi:10.1016/j.advwatres.2007.06.004, 2007.

Schulte, J. A.: Cumulative areawise testing in wavelet analysis and its application to geophysical time series, Nonlin. Processes Geophys., 23, 45–57, doi:10.5194/npg-2345-2016, 2016.

Schulte, J. A., Duffy, C., and Najjar, R. G.: Geometric and topological approaches to significance testing in wavelet analysis, Nonlin. Processes Geophys., 22, 139–156, doi:10.5194/npg-22-139-2015, 2015.

She, D. L., Liu, D. D., Peng, S. Z., and Shao ,M. A.: Multiscale influences of soil

properties on soil water content distribution in a watershed on the Chinese Loess Plateau, Soil Sci., 178, 530–539, doi: 10.1097/SS.0000000000000021, 2013.

She, D. L., Zheng, J. X., Shao, M. A., Timm, L. C., and Xia, Y. Q.: Multivariate empirical mode decomposition derived multi-scale spatial relationships between saturated hydraulic conductivity and basic soil properties, Clean-Soil Air Water, doi: 10.1002/clen.201400143, 2015.

Si, B. C.: Spatial scaling analyses of soil physical properties: A review of spectral and wavelet methods, Vadose Zone J., 7, 547–562, doi: 10.2136/vzj2007.0040, 2008.

Si, B. C. and Zeleke, T. B.: Wavelet coherency analysis to relate saturated hydraulic properties to soil physical properties, Water Resour. Res., 41, W11424, doi:10.1029/2005WR004118, 2005.

Tang, C. L. and Piechota, T. C.: Spatial and temporal soil moisture and drought variability in the Upper Colorado River Basin, J. Hydrol., 379, 122–135, doi: 10.1016/j.jhydrol.2009.09.052, 2009.

Torrence, C. and Compo, G. P.: A practical guide to wavelet analysis, Bull. Am. Meteorol. Soc., 79, 61–78, doi: 10.1175/1520-0477(1998)079<0061:apgtwa>2.0.co;2, 1998.

Torrence, C. and Webster, P. J.: Interdecadal changes in the ENSO-monsoon system, J. Clim., 12, 2679–2690, doi: 10.1175/1520-0442(1999)012<2679:ICITEM>2.0.CO;2, 1999.

Yan, R. and Gao, R. X.: A tour of the Hilbert–Huang transform: an empirical tool for signal analysis, IEEE Instrum. Meas. Mag., 10, 40–45, doi:

514 10.1109/MIM.2007.4343566, 2007.

## Figure captions

**Figure 1**. (a) Stationary and (b) non-stationary series of response variables ($y$ for stationary and $z$ for non-stationary case) encompassing five cosine waves ($y_1$ to $y_5$ for stationary and $z_1$ to $z_5$ for non-stationary case) with different dimensionless scales.

**Figure 2.** Multiple wavelet coherence (a) between response variable $y$ and predictor variables $y_2$ and $y_4$; (b) between response $y$ and predictors $y_2$, $y_3$, and $y_4$; (c) between response z and predictors $z_2$ and $z_4$; and (d) between response z and predictors $z_2$, $z_3$, and $z_4$. The artificial data series ($y$) encompasses five cosine waves ($y_1$, $y_2$, $y_3$, $y_4$, and $y_5$) with different scales for the stationary case, and the artificial data series ($z$) encompasses five cosine waves ($z_1$, $z_2$, $z_3$, $z_4$, and $z_5$) with different scales for the non-stationary case. The predictor variables, connected by a hyphen, are shown in the top right corner of each subplot. Thin solid lines demarcate the cones of influence, and thick solid lines show the 95% confidence levels.

**Figure 3.** Multiple wavelet coherence (a) between $y$ and $y_2h_0$ and $y_4$; (b) between $y$ and $y_2$ and $y_4h_0$; (c) between $z$ and $z_2h_0$ and $z_4$; and (d) between $z$ and $z_2$ and $z_4h_0$. The variables $y_2h_0$ (or $z_2h_0$) and $y_4h_0$ (or $z_4h_0$) refer to the new series of $y_2$ (or $z_2$) and $y_4$ (or $z_4$), in which the second half are replaced by 0.

**Figure 4.** Multiple wavelet coherence of an artificial data series ($z$) encompassing five cosine waves ($z_1$, $z_2$, $z_3$, $z_4$, and $z_5$) with different scales and (a) $z_2$ and noised $z_2$, (b) $z_2$ and noised $z_4$, and (c) $z_2$, $z_4$, and noised $z_4$ for the non-stationary case. $z_2wn$ ($z_4wn$), $z_2mn$ ($z_4mn$), and $z_2sn$ ($z_4sn$) indicate weakly, moderately, and strongly noised $z_2$ ($z_4$) series, respectively. Weakly, moderately, and strongly noised series are correlated with

original series, having with correlation coefficients of 0.9, 0.5, and 0.1, respectively.

**Figure 5.** Multiple spectral coherence (MSC) of an artificial data series ($y$ or $z$) encompassing five cosine waves ($y_1$ to $y_5$; or $z_1$ to $z_5$) with different scales and (a) two ($y_2$ and $y_4$; or $z_2$ and $z_4$) or three ($y_2$, $y_3$, and $y_4$; or $z_2$, $z_3$, and $z_4$) data series, and (b) two ($y_2$ and $y_4$; or $z_2$ and $z_4$) data series when the second half of one data series are replaced by 0. The variables $y_2h_0$ (or $z_2h_0$) and $y_4h_0$ (or $z_4h_0$) refer to the new series of $y_2$ (or $z_2$) and $y_4$ (or $z_4$) in which the second half are replaced by 0.

**Figure 6.** Multiple correlation coefficient between multivariate empirical mode decomposition ($MCC_{memd}$) of an artificial series ($y$ or $z$) and (a) two ($y_2$ and $y_4$; or $z_2$ and $z_4$) or three ($y_2$, $y_3$, and $y_4$; or $z_2$, $z_3$, and $z_4$) data series, and (b) two ($y_2$ and $y_4$; or $z_2$ and $z_4$) data series when the second half of one data series are replaced by 0.The variables $y_2h_0$ (or $z_2h_0$) and $y_4h_0$ (or $z_4h_0$) refer to the new series of $y_2$ (or $z_2$) and $y_4$ (or $z_4$) in which the second half are replaced by 0.

**Figure 7.** Multiple wavelet coherence between evaporation ($E$) from water surfaces and meteorological factors ((a) relative humidity and mean temperature and (b) relative humidity, mean temperature, and sun hours) at Changwu site in Shaanxi, China.

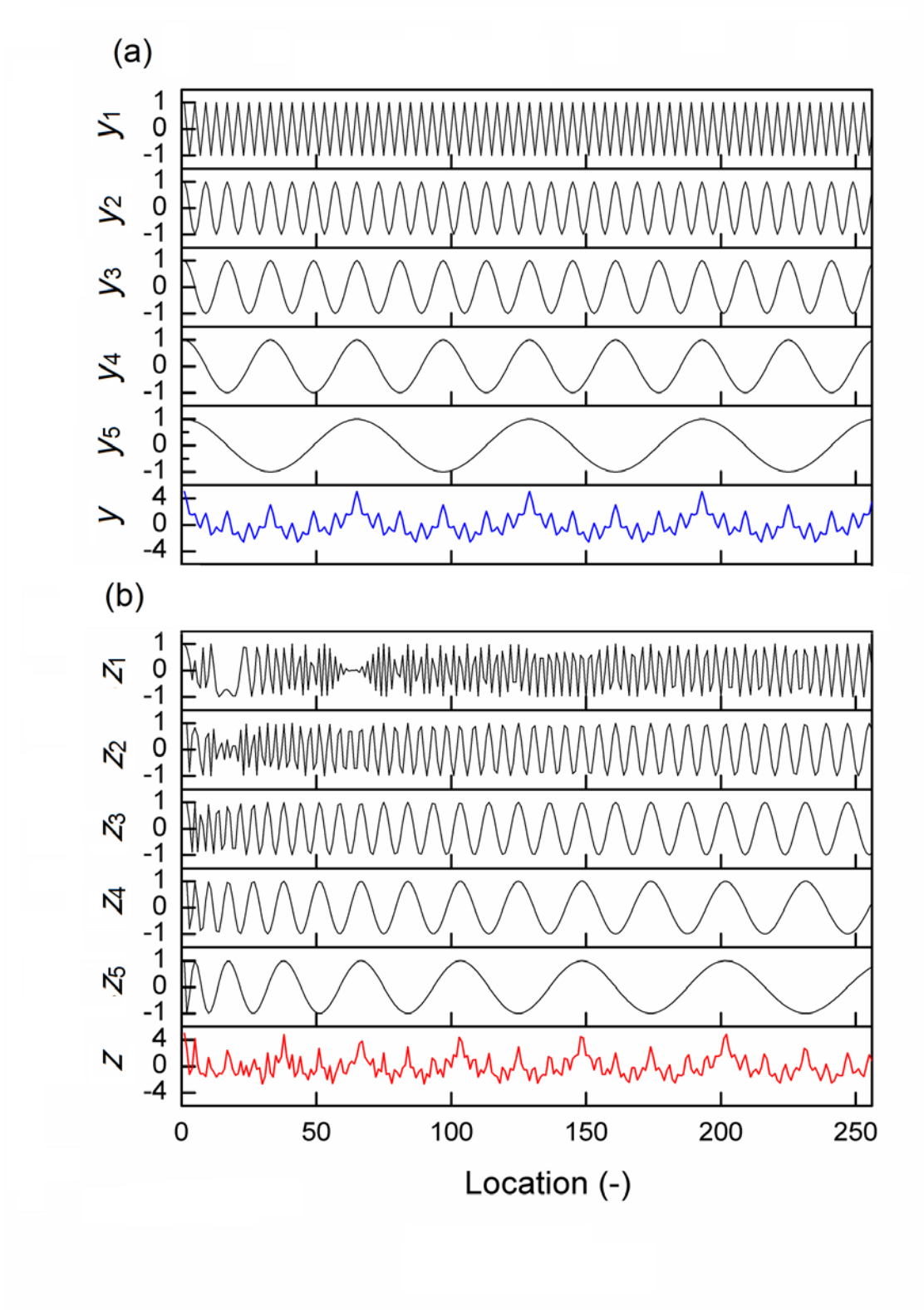


**Figure 1**. (a) Stationary and (b) non-stationary series of response variables ($y$ for stationary and $z$ for non-stationary case) encompassing five cosine waves ($y_1$ to $y_5$ for stationary and $z_1$ to $z_5$ for non-stationary case) with different dimensionless scales.

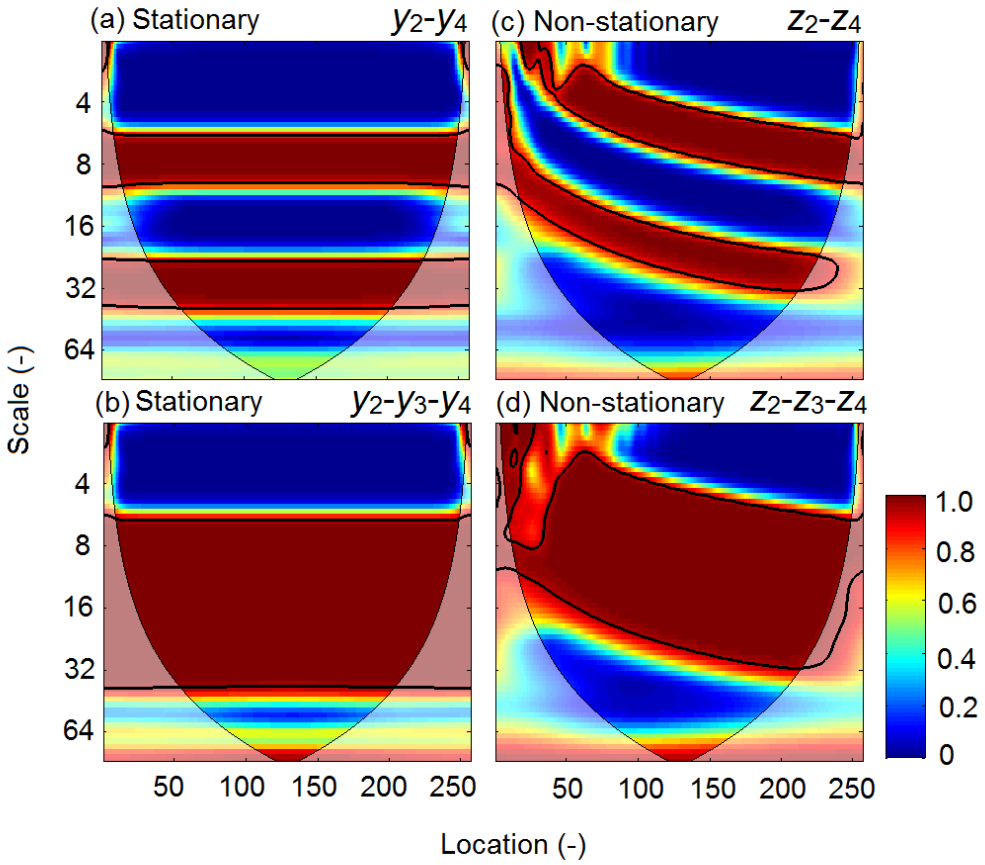


**Figure 2.** Multiple wavelet coherence (a) between response variable $y$ and predictor variables $y_2$ and $y_4$; (b) between response $y$ and predictors $y_2$, $y_3$, and $y_4$; (c) between response z and predictors $z_2$ and $z_4$; and (d) between response z and predictors $z_2$, $z_3$, and $z_4$. The artificial data series ($y$) encompasses five cosine waves ($y_1$, $y_2$, $y_3$, $y_4$, and $y_5$) with different scales for the stationary case, and the artificial data series ($z$) encompasses five cosine waves ($z_1$, $z_2$, $z_3$, $z_4$, and $z_5$) with different scales for the non-stationary case. The predictor variables, connected by a hyphen, are shown in the top right corner of each subplot. Thin solid lines demarcate the cones of influence, and thick solid lines show the 95% confidence levels.

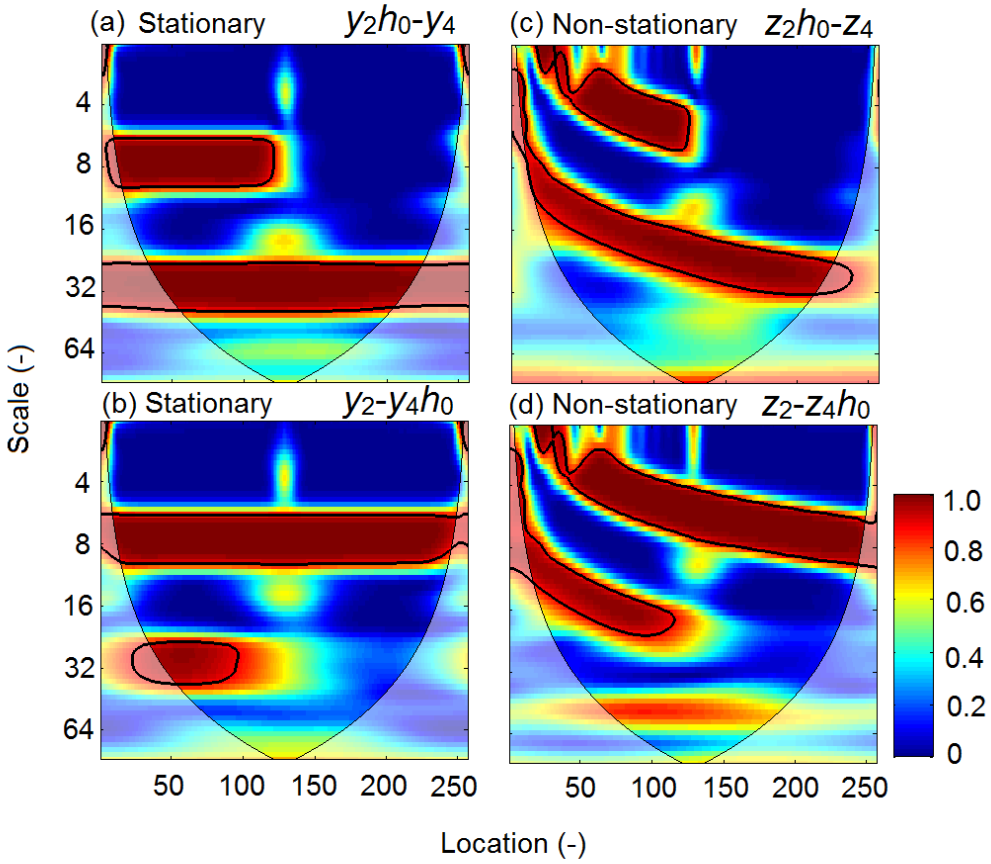


**Figure 3.** Multiple wavelet coherence (a) between $y$ and $y_2h_0$ and $y_4$; (b) between $y$ and $y_2$ and $y_4h_0$; (c) between $z$ and $z_2h_0$ and $z_4$; and (d) between $z$ and $z_2$ and $z_4h_0$. The variables $y_2h_0$ (or $z_2h_0$) and $y_4h_0$ (or $z_4h_0$) refer to the new series of $y_2$ (or $z_2$) and $y_4$ (or $z_4$), in which the second half are replaced by 0.

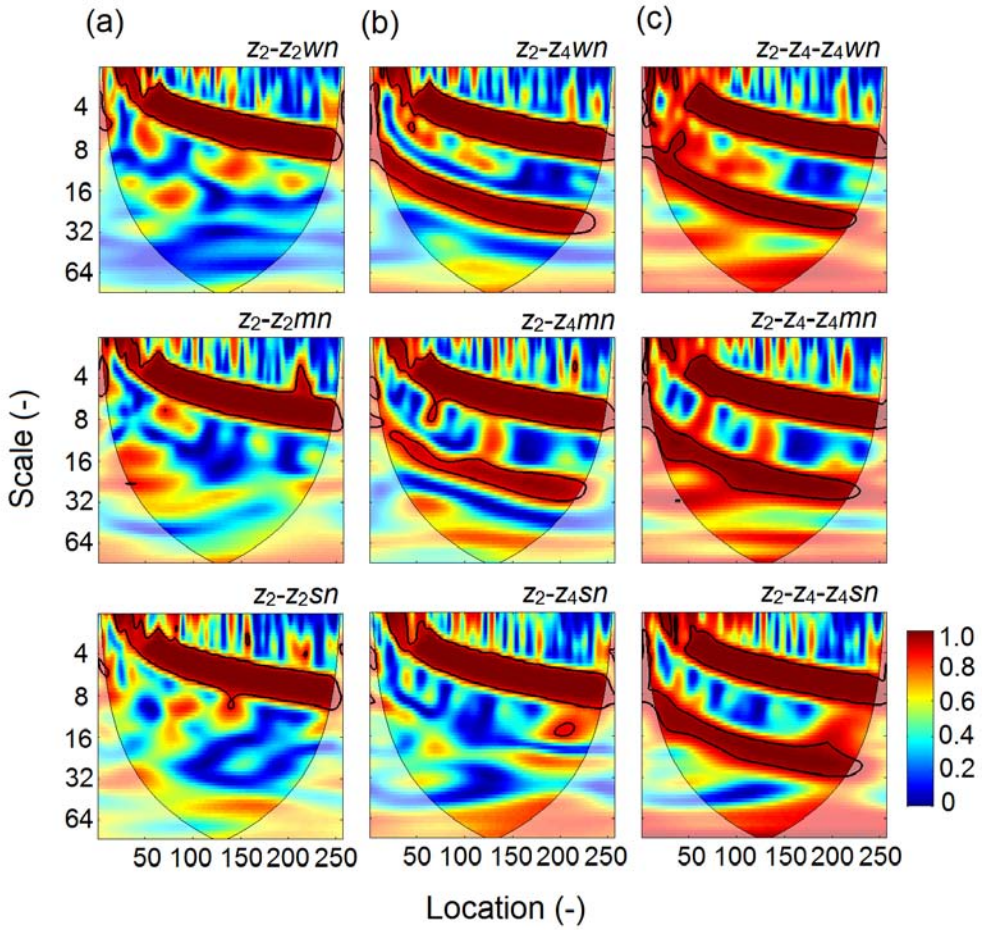


**Figure 4.** Multiple wavelet coherence of an artificial data series ($z$) encompassing five cosine waves ($z_1$, $z_2$, $z_3$, $z_4$, and $z_5$) with different scales and (a) $z_2$ and noised $z_2$, (b) $z_2$ and noised $z_4$, and (c) $z_2$, $z_4$, and noised $z_4$ for the non-stationary case. $z_2wn$ ($z_4wn$), $z_2mn$ ($z_4mn$), and $z_2sn$ ($z_4sn$) indicate weakly, moderately, and strongly noised $z_2$ ($z_4$) series, respectively. Weakly, moderately, and strongly noised series are correlated with original series, having with correlation coefficients of 0.9, 0.5, and 0.1, respectively.

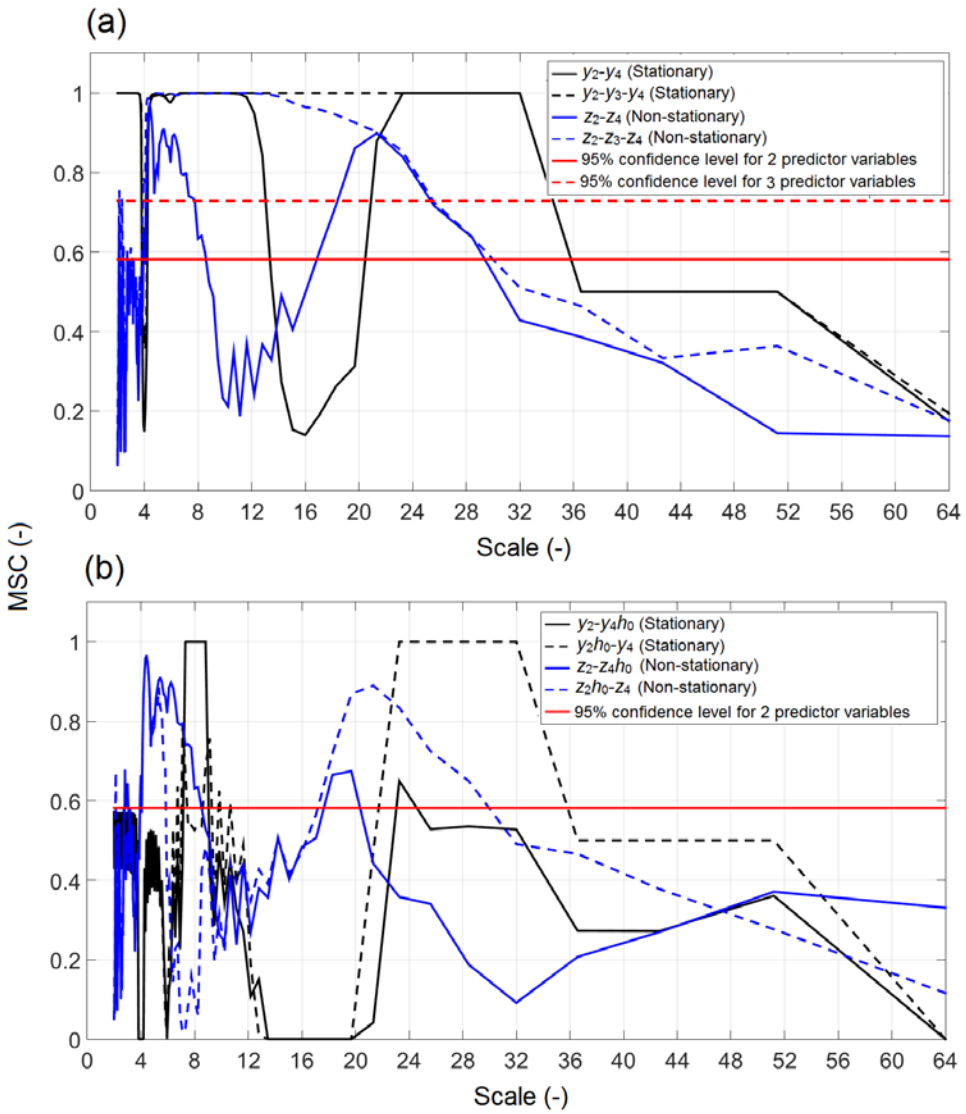


**Figure 5.** Multiple spectral coherence (MSC) of an artificial data series ($y$ or $z$) encompassing five cosine waves ($y_1$ to $y_5$; or $z_1$ to $z_5$) with different scales and (a) two ($y_2$ and $y_4$; or $z_2$ and $z_4$) or three ($y_2$, $y_3$, and $y_4$; or $z_2$, $z_3$, and $z_4$) data series, and (b) two ($y_2$ and $y_4$; or $z_2$ and $z_4$) data series when the second half of one data series are replaced by 0. The variables $y_2h_0$ (or $z_2h_0$) and $y_4h_0$ (or $z_4h_0$) refer to the new series of $y_2$ (or $z_2$) and $y_4$ (or $z_4$) in which the second half are replaced by 0.

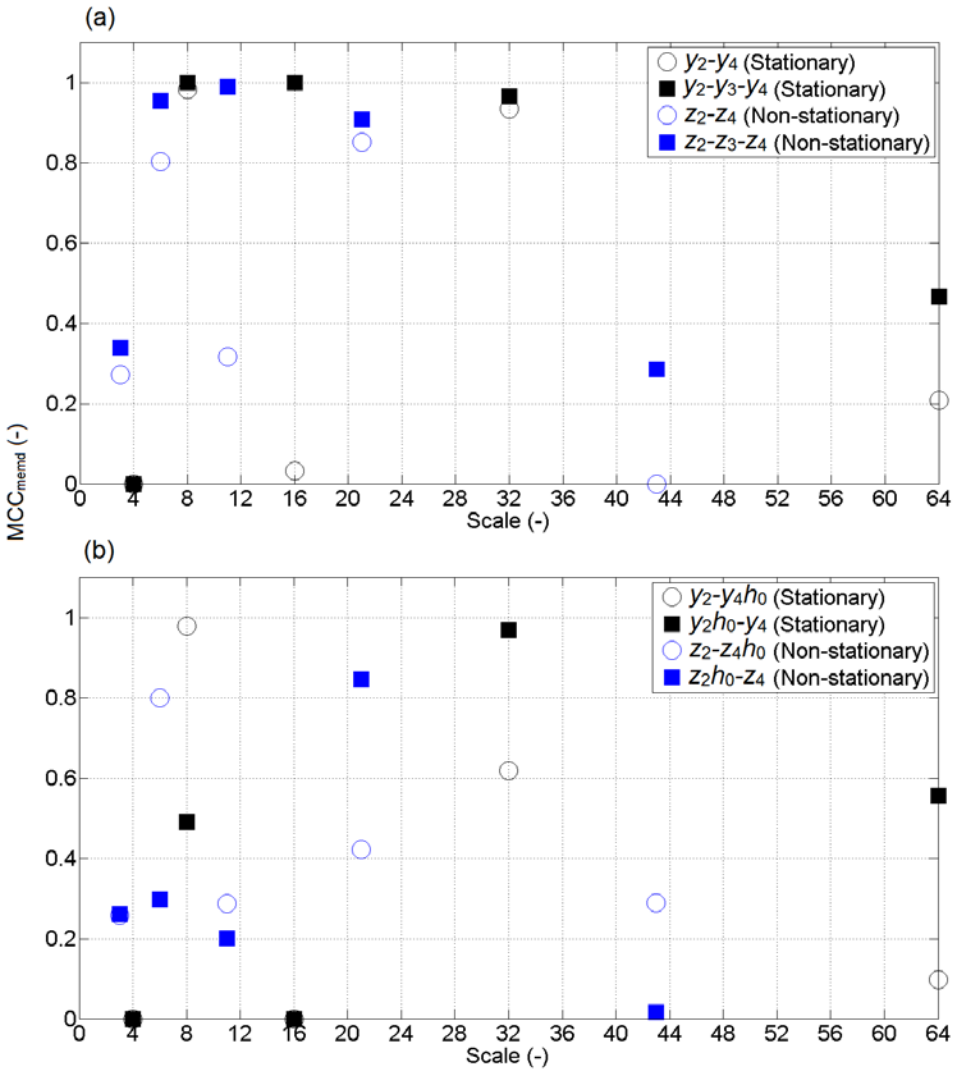


**Figure 6.** Multiple correlation coefficient between multivariate empirical mode decomposition ($MCC_{memd}$) of an artificial series ($y$ or $z$) and (a) two ($y_2$ and $y_4$; or $z_2$ and $z_4$) or three ($y_2$, $y_3$, and $y_4$; or $z_2$, $z_3$, and $z_4$) data series, and (b) two ($y_2$ and $y_4$; or $z_2$ and $z_4$) data series when the second half of one data series are replaced by 0.The variables $y_2h_0$ (or $z_2h_0$) and $y_4h_0$ (or $z_4h_0$) refer to the new series of $y_2$ (or $z_2$) and $y_4$ (or $z_4$) in which the second half are replaced by 0.

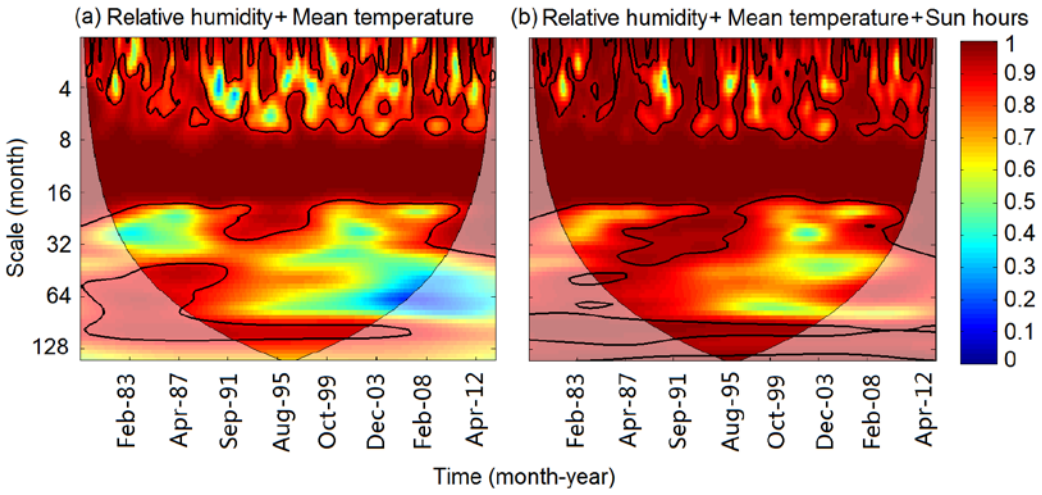


**Figure 7.** Multiple wavelet coherence between evaporation (*E*) from water surfaces and meteorological factors ((a) relative humidity and mean temperature and, (b) relative humidity, mean temperature, and sun hours) at Changwu site in Shaanxi, China.